Energy optimization control of extended-range hybrid combine harvesters based on quasi-cycle power demand estimation

Shuofeng Weng,[1,2] Chaochun Yuan,[3,4,5] Youguo He,[3] Jie Shen,[6] Lizhang Xu,[4,5] Zhihao Zhu,[1] Qiuye Yu,[7] Xiaowei Yang[3]

[1]School of Agricultural Engineering, Jiangsu University, Zhenjiang, China; [2]Faculty of Agricultural Engineering, Jiangsu University, Zhenjiang, China; [3]Automotive Engineering Research Institute, Jiangsu University, Zhenjiang, China; [4]Key Laboratory for Theory and Technology of Intelligent Agriculture Machinery and Equipment, Jiangsu University, Zhenjiang, China; [5]Jiangsu Province and Education Ministry Co-sponsored Synergistic Innovation Center of Modern Agricultural Equipment, Jiangsu University, Zhenjiang, China; [6]University of Michigan-Dearborn, Dearborn MI, USA; [7]China Automotive Technology & Research Center Co. Ltd., Tianjin, China

Abstract

This study develops an energy management strategy (EMS) for hybrid combine harvesters to address fluctuating power demands in agricultural operations. By segmenting harvesting processes into quasi-periodic cycles linked to machine dynamics, the method integrates component-specific power models (header, conveyor, drum) for accurate energy estimation. Real-time feed rate adjustments are achieved through dynamic responses of critical components, optimizing cycle duration and power allocation. A genetic algorithm synchronizes energy distribution and cycle timing to minimize fuel consumption. Validated *via* AMESim/Simulink co-simulation with dual engine models, the strategy reduces fuel use by 21.1% compared to conventional systems. Key innovations include quasi-periodic load segmentation, component-response-based feed rate prediction, and GA-driven multi-objective optimization. The approach enhances adaptability to variable harvesting conditions, offering a scalable framework for energy-efficient electrification in agriculture. Results demonstrate significant potential for hybrid systems in reducing operational costs and emissions while maintaining productivity under dynamic workloads.

Correspondence: Chaochun Yuan, Automotive Engineering Research Institute, Jiangsu University, No.301, Xuefu Road, Jingkou District, Zhenjiang, Jiangsu, 212013, China.
E-mail: yuancc_78@163.com
Qiuye Yu, China Automotive Technology & Research Center Co. Ltd., No. 3, Wanhui Road, Xiqing District, Tianjin, 300300, China.
E-mail: yuqiuye@catarc.ac.cn

Key words: combines; hybrids; quasi-cycle processes; energy management strategy.

Received: 17 November 2024.
Accepted: 22 May 2025.

Journal of Agricultural Engineering 2025; LVI:
doi:10.4081/jae.2025.1819

Introduction

By 2020, China's rice mechanization harvesting level had reached 90%, with approximately 1.6 million rice combine harvesters in operation (Xuegeng *et al.*, 2020; Deng *et al.*, 2020; Hu *et al.*, 2024). While mechanized harvesting significantly improves efficiency, the energy consumption of combine harvesters has become a pressing concern (Lang *et al.*, 2018; Savickas *et al.*, 2020; Kotenko, 2022; Chai *et al.*, 2024). Hybrid configurations, widely used in the automotive industry for their energy efficiency, present a promising solution. Developing effective hybrid energy management strategies for harvesting operations can further enhance the energy-saving potential of hybrid harvesters (Schmid *et al.*, 2019; Guo *et al.*, 2019; Shi *et al.*, 2016).

Existing research classifies hybrid energy management strategies into three main categories: rule-based strategies, transient optimization strategies, and global optimization strategies (Sun *et al.*, 2023; Zhu *et al.*, 2022).

The rule-based strategy is designed based on key engine and motor characteristics, such as the manifold absolute pressure (MAP) diagram. It also considers factors like the battery's state of charge (SoC), torque, and speed demand to achieve optimal efficiency (Wang *et al.*, 2018). Zhu *et al.* (2021) further refined this approach by using the battery SoC as a benchmark for mode-switching and applying dynamic programming to optimize energy consumption. Building on these advancements, Shi *et al.* (2023) introduced an integrated rule-based (IRB) strategy that incorporates a reference SoC curve and adaptive SoC adjustments. This approach ensures a linear SoC decrease over driving distance, culminating in a minimum SoC at the journey's end, resembling the results of the dynamic programming (DP) strategy. While the rule-based strategy is easy to implement, its application in hybrid harvesters presents challenges due to fluctuating energy demands. As a result, achieving high fuel efficiency across various working conditions with a simple rule-based strategy is difficult, highlighting the need for a more adaptive approach.

The transient optimization strategy focuses on stabilizing the SoC while minimizing fuel consumption. A key example is the equivalent consumption minimum strategy (ECMS), which optimizes energy use by dynamically adjusting the engine's operating points to match transient power demands (Shi *et al.*, 2021). Zhu *et al.* (2021) proposed an adaptive-ECMS strategy that adjusts to SoC variations, ensuring efficient charge-discharge cycles. Additionally, the Cost Optimization for Finite Horizon strategy integrates future driving condition information from vehicle-to-vehicle technology to optimize fuel consumption. While transient optimization strategies are robust and adaptable to changing power demands, their real-time power tracking approach, although beneficial for SoC stability, may limit overall power efficiency when applied to hybrid harvesters with highly dynamic operational conditions. Global optimization strategies have gained increasing attention for their ability to allocate power sources optimally over an entire operation cycle. This approach applies optimal control theory to predefined working conditions to minimize fuel consumption (Ali and Moulik, 2022; Wang *et al.*, 2023; Zhang *et al.*, 2019). Recent studies have explored advanced adaptations, such as Shi's fuzzy adaptive method for the PMP-based optimal approach, which incorporates real-time traffic data, including average velocity and velocity fluctuations, to enhance optimization (Yu *et al.*, 2013). However, despite its effectiveness, global optimization has inherent limitations. It requires significant computational resources, making real-time implementation challenging. Additionally, this strategy depends on pre-acquired operating condition data, which may not always align with real-world variations. Given the complexity of harvester operations, obtaining accurate pre-operational data is difficult, potentially reducing the strategy's robustness and practicality. Most research on hybrid energy management focuses on optimizing hybrid vehicles based on real-time or predicted power demand. However, these approaches often fail to meet the specific energy management challenges of hybrid harvesters (Yang *et al.*, 2021; Liu *et al.*, 2021). Unlike hybrid vehicles, harvesters operate in distinct phases, including harvesting, transferring, and grain unloading, each with unique and highly dynamic power demands. Current energy management strategies struggle to model and manage these variations effectively. However, the harvesting process follows a regular pattern, allowing it to be segmented into discrete phases. Developing energy management strategies tailored to each phase and considering their specific power demand characteristics can significantly improve the overall energy efficiency of hybrid harvesters. To address these challenges, this study introduces an innovative energy management strategy based on a quasi-cycle operation state demand model. This model captures the periodicity of key harvester processes, including harvesting, material transfer, and grain unloading. It integrates feed rate estimation, refined through the dynamic responses of critical components, with a genetic algorithm to optimize the fuel consumption of the range extender. By aligning energy management with the operational characteristics of hybrid harvesters, this approach maximizes energy savings and provides a more effective solution tailored to their specific requirements.

The remainder of this paper is organized as follows: a section presenting the hybrid combine harvester model design; a paragraph detailing power demand modeling based on quasi-periodic processes; a paragraph outlining the power management optimization strategy utilizing a genetic algorithm; a paragraph describing the simulation experiment design; and the final section discussing the results and key findings.

Hybrid combine harvester model design

During harvester operation, the harvesting and travel components experience complex load variations, characterized by frequent and significant fluctuations in power demand. To mitigate the impact of these energy fluctuations on the engine under varying conditions, the mechanical coupling between the engine and the component drive system is eliminated.

The typical hybrid harvester energy system consists of an engine, generator, and motor drive. This system adopts a distributed topology, where drive motors are installed near each component. This configuration shortens the drive chain, reduces transmission energy losses, and improves overall efficiency. Given the frequent changes in power demand across different operating conditions, independent motors drive the harvesting, travel, and grain unloading components. This design enables precise energy matching for each operational state, ensuring optimal performance under varying workloads.

The WORLD 4LZ-9A agricultural combine was selected as the prototype for modification. Its original technical specifications and parameters of the retrofitted energy unit are systematically presented in Appendices A and B. The parameters in Appendix A were provided by engineers from Jiangsu World Electromechanical Company, while Appendix B presents the component selection results based on the original requirements of the entire machine and subsystems, with battery parameters sourced from Guangdong Snova Technologies Co., Ltd., motor parameters from Suzhou Sigma Technologies Co., Ltd., and range extender parameters from Guangxi Yuchai Technologies Co., Ltd., where partial parameters in Appendix B are also documented in a previous work which has been published (Zhu *et al.*, 2023).

Overview of system structure

The initial configuration of the prototype harvester is illustrated in Figure 1, depicting the fuel-driven power transmission system where the engine centrally drives all components through belt-pulley linkages (Xu *et al.*, 2020). The retrofitted hybrid configuration, as shown in Figure 2, adopts a distributed electromechanical drive system. This modified architecture replaces the centralized belt-pulley transmission with eight dedicated motor-driven modules: (1) cutting table, (2) conveying chute, (3) threshing drum, (4) cleaning device, (5) grain elevator, (6) travel drive, (7) residue chopper, and (8) discharge auger. By systematically decomposing the power transmission system, this design eliminates 80% of the original belt drives while enabling precise power distribution and improved operational efficiency.

Modeling of hybrid power components

The energy supply system examined in this study comprises an engine, generator, and battery, all of which exhibit nonlinear dynamic characteristics that are difficult to model with precision. To facilitate analysis, the study employs an equivalent model to simplify the energy consumption characteristics. In this approach, the engine and generator are treated as a single integrated system, while the battery's dynamic efficiency characteristics are approximated using a fixed efficiency value. This simplification enables a more computationally efficient and manageable assessment of the energy supply system's performance (Wang *et al.*, 2021).

The efficiency of engine and motor is given by:

$$\begin{cases} W_{\mathrm{che}} = \dot{m}_{\mathrm{f}}(\omega_{\mathrm{E}}, T_{\mathrm{E}}) H_{\mathrm{lhv}} \\ W_G = U_G \bullet I_G \\ \eta_{\mathrm{E\_G}} = W_G / W_{\mathrm{che}} \end{cases}$$

where: W_{che} is the fuel chemical energy of the engine, $\dot{m}_f$ is the fuel consumption rate, ω_E is the engine speed, T_E is the engine torque, H_{lhv} is the fuel calorific value, W_G is the power of the generator, h_{E_G} is the efficiency of the engine, U_G is the voltage of the generator, I_G is the current of generators.

Power demand modeling based on quasi periodic processes

The power demand of agricultural harvesters is significantly more complex than that of vehicles due to the numerous driven components and diverse operating conditions. In particular, the requirements for speed and drive power across a harvester's har-

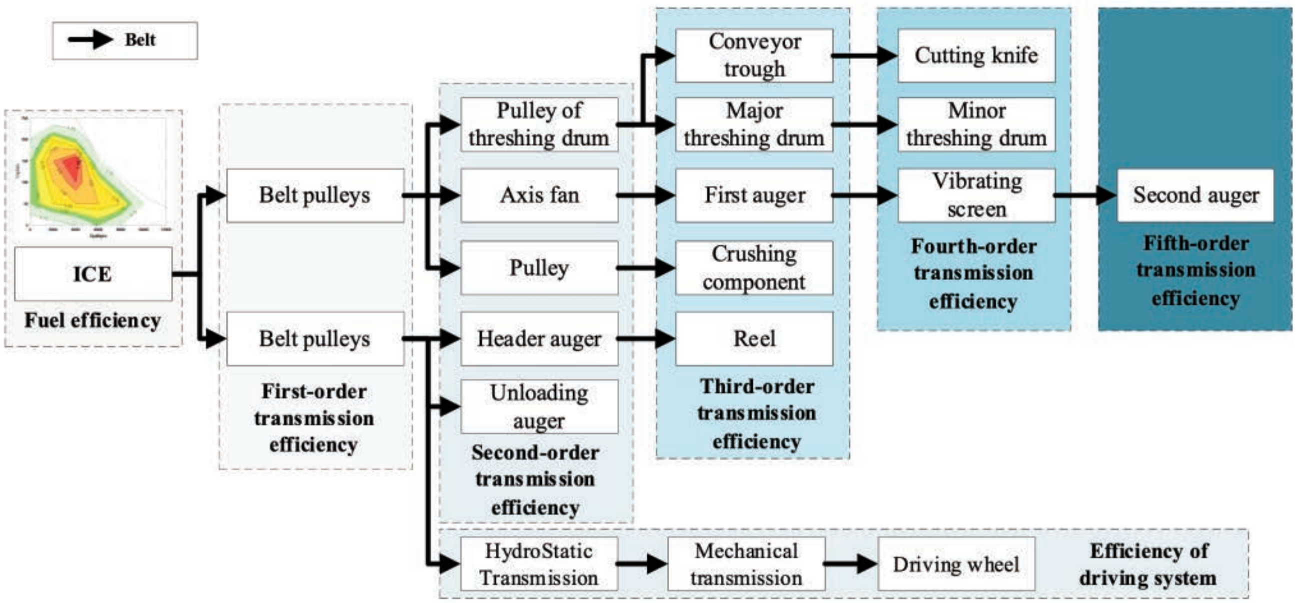

Figure 1. Typical configuration of a fuel-driven harvester.

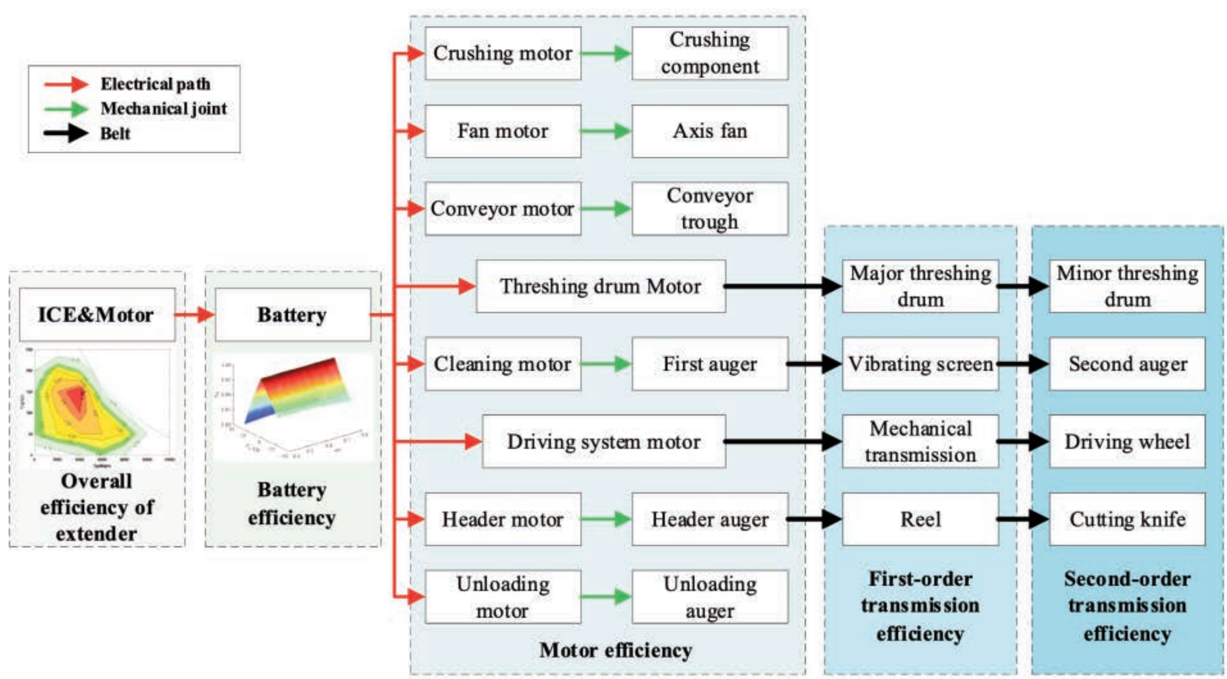

Figure 2. Schematic diagram of the hybrid harvester configuration.

vesting, threshing, and sorting mechanisms fluctuate considerably based on varying operational needs. A detailed modeling and analysis of the energy consumption characteristics of these distinct components under different working conditions are essential. Additionally, torque demand during operation is strongly influenced by factors such as feed rate. Despite these complexities, it is possible to estimate the power demand of harvesters with reasonable accuracy. This study examines a harvester's typical workflow, segmenting its standard operational cycle into four working conditions: harvesting, full-load transferring, unloading, and empty-load transferring. This classification reflects the sequential process inherent in harvester operations and provides a structured framework for energy demand estimation.

Components power demand in quasi periodic processes

To accommodate the capacity limitations of the grain tank, a harvester must perform multiple grain unloading operations to complete the harvesting of a crop region. To facilitate a more detailed analysis of the power demand characteristics of different components, the harvester's operational process is simplified into one or more quasi-cycle processes. These quasi-cycle processes consist of four stages: harvesting, full-load transferring, unloading, and empty-load transferring. A typical representation of such a quasi-cycle process is illustrated in Figure 3. This simplification helps in understanding the power demand variations across different components throughout the harvester's operation (Luo *et al.*, 2022). In a typical quasi-cycle process, each component of the combine works in different states, shown in Table 1.

Components power demand modeling

The component demands listed in Table 1 are modeled based on various harvester parameters to determine the power requirements of each component during the quasi-periodic process. To simplify the calculations, the rotational inertia of gears and shafts is disregarded. Additionally, the effects of mechanical deformation and other external factors on the load are not considered. For this analysis, the feeding process is assumed to be uniform and continuous.

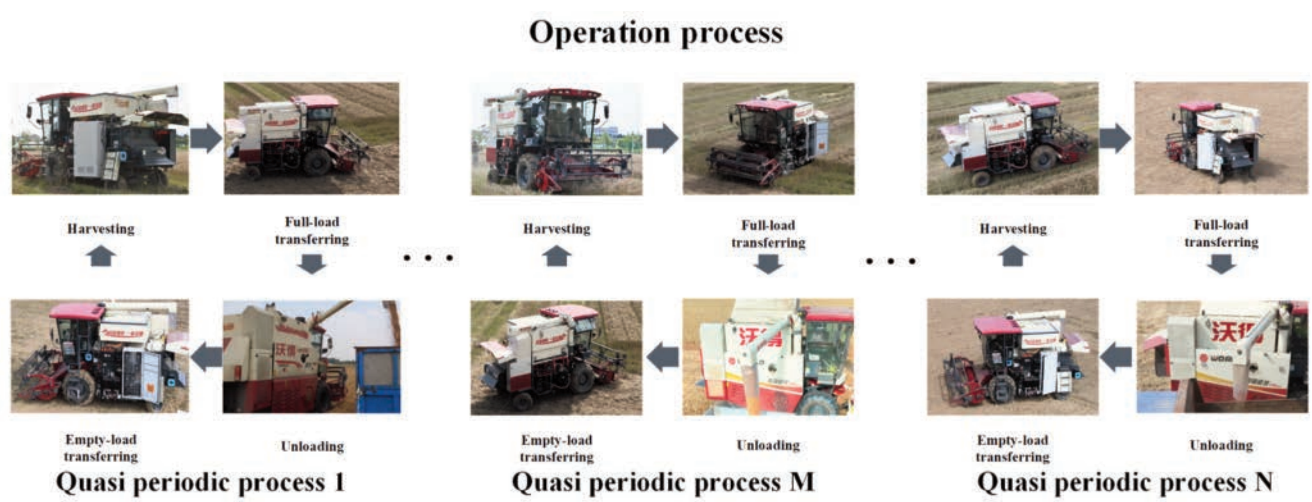

Figure 3. A typical cycle of harvester operation.

Table 1. Energy consumption status of components in a typical quasi-cycle process.

Components work or not conditions	Harvesting	Full-load transferring	Unloading	Empty-load transferring
Header	Yes	No	No	No
Conveyor trough	Yes	No	No	No
Threshing drum	Yes	No	No	No
Cleaning components	Yes	No	No	No
Auger	Yes	No	No	No
Crushing components	Yes	No	No	No
Driving components	Yes	Yes	No	Yes
Grain unloading components	No	No	Yes	No
Heat dissipation components	Yes	Yes	Yes	Yes

Power demand of harvesting system

Power demand of header

The typical header model, which consists of the cutter, sheave wheel, and churn, exhibits active torque in three distinct segments during operation. The first segment corresponds to the idling friction torque, observed when the header operates under no-load conditions. The second segment represents the torque required for paddle paddling, cutter cutting, and churn pushing operations. The magnitude of this torque is closely related to the real-time feed rate of the harvester and is modeled as a linear function of the feed rate, as detailed in Sun *et al*. (2022). The third segment accounts for the rotational moments of inertia, as discussed in Chen *et al*. (2017). These components are collectively integrated into the simplified power demand model of the header, which is presented in this paper as Eq. (1).

$$P_g = \left(M_{ci} + M_{pi} + M_{mi} + k_c q + k_p q + k_m q + \left(\frac{J_c}{i_c} + \frac{J_m}{i_m}\right)\frac{d\omega_{gi}}{dt} \right)\omega_{gi} \quad \text{(Eq. 1)}$$

where: P_g is the power demand, M_{pi} is the idling friction torque of the paddle wheel, M_{ci} is the idling friction torque of the cutting knife, M_{mi} is the idling friction torque of the header churn, i_c, i_m are the transmission ratio from the main shaft to the paddle wheel and the churn, J_c is the rotational inertia of the paddle wheel, ω_{gi} is the input speed of the driving shaft of the header, J_m is the rotational inertia of the churn, k_c, k_p, k_m are the feeding coefficient of the cutter, paddle wheel and header churn.

Power demand of conveying trough

The active torque of the conveyor trough is determined by three key elements: the idling friction moment, the crop transport moment, and the inertia of the conveyor trough. The crop transport moment is influenced by two factors: the mass of the crop on the conveyor belt and the inclination of the conveyor belt, as detailed in Chen *et al.* (2017). The relationship between the crop mass on the conveyor belt and the feed rate is approximated as linear. This paper presents a simplified power demand model for the conveyor trough, formulated in Eq. (2).

$$P_s = \left(M_{bi} + k_{sq} q + \frac{J_b + k_{sm} \times q}{i_b}\frac{d\omega_b}{dt} \right)\omega_b \quad \text{(Eq. 2)}$$

where: P_s is the power demand of the conveyor trough, M_{bi} is the idling friction torque of the conveyor trough, i_b is the ratio of the input shaft to the conveyor trough, R_b is the radius of the active wheel, J_b is the rotational inertia of the conveyor trough, ω_b is the rotation speed of the input shaft, k_{sq} is the feed rate coefficient of the conveying moment, k_{sm} is the feed rate coefficient of the mass of the crop.

Power demand of threshing drum

Similarly, the active torque of the threshing drum consists of three key components: the idling resistance torque, the torque required for pushing the grain, and the drum's moment of inertia. The idling torque primarily arises from mechanical friction resistance and air resistance caused by the drum blast. This aspect of the drum's operation is modeled based on existing literature (Yun *et al.*, 2010) and is formulated in Eq. (3).

$$M_{rk} = A + B\omega_r^2 \quad \text{(Eq. 3)}$$

where: ω_r is the rotation speed of the drum, A is the mechanical friction resistance moment, B is the blast resistance coefficient. The crop acceleration load moment enables the threshing drum to accelerate the crop to a specific speed. The required torque is determined based on existing literature (Yun *et al.*, 2010) and is formulated in Eq. (4).

$$M_{rv} = \frac{1}{2} q \frac{\lambda + \delta}{1 + \delta} R_r^2 \omega_r \quad \text{(Eq. 4)}$$

where: R_r is the equivalent radius, λ is the ratio of tangential speed of the crop to the linear speed of the drum rotation, δ is the seed-straw ratio.

According to prevailing research, a proportional relationship exists between grain acceleration and the total working moment during the operation of the threshing drum, as outlined in Yun *et al.* (2010). Consequently, the working frictional resistance moment of the drum can be expressed as:

$$M_{rw} = \frac{M_{rv}}{1 - f} \quad \text{(Eq. 5)}$$

where: f is the rubbing factor.

The moment of inertia of the threshing drum is shown in Eq. (6).

$$M_{rg} = J_r \frac{d\omega_r}{dt} \quad \text{(Eq. 6)}$$

where: J_r is the rotational inertia of the threshing drum.

In summary, the power demand model for the threshing drum is:

$$P_t = \left[J_r \frac{d\omega_r}{dt} + A + B\omega_r^2 + \frac{qR_r^2\omega_r(\lambda + \delta)}{2(1+\delta)(1-f)} \right]\omega_r \quad \text{(Eq. 7)}$$

Power demand of cleaning components

The active torque of the cleaning device consists of several components: the fan rotation torque, the torque required to overcome the sieve plate's no-load friction, the torque needed to move the crop on the sieve plate, and the moment of inertia associated with the sieve plate's acceleration. The operational torque of the sieve plate exhibits a linear correlation with the harvester's feed rate, allowing for the formulation of the cleaning device's kinetic equation, as detailed in Eqs. (8) and (9).

$$P_t = \left[J_r \frac{d\omega_r}{dt} + A + B\omega_r^2 + \frac{qR_r^2\omega_r(\lambda + \delta)}{2(1+\delta)(1-f)} \right]\omega_r \quad \text{(Eq. 8)}$$

$$q_s = q \times \delta \quad \text{(Eq. 9)}$$

where: P_q is the power demand of the cleaning device, M_{si} is the idling torque required sieve plate and fan, J_s is the rotational inertia of the sieve plate, q_s is the seed feeding amount, R_s is the radius of the drive wheel, t_s is the residence time of the seed on the sieve plate, k_s is the feeding coefficient of sieve plate, ω_s is the shaft rotation speed, i_s is the transmission ratio from the input shaft to the cleaning sieve, q_s is the grain feed rate, δ is the ratio of grain.

Power demand of crushing device

For the crushing device, its active torque primarily consists of idling torque and the torque required for straw crushing. The torque needed for straw crushing exhibits a linear relationship with the harvester's feed rate, enabling the formulation of the crushing device's kinetic equation, as represented in Eq. (10).

$$P_f = \left[M_{fi} + k_f q_s + J_f \frac{d\omega_f}{dt} \right] \omega_f \quad \text{(Eq. 10)}$$

where: P_f is the power demand of the crushing device, M_{fi} is the idling torque of crushing device, J_f is the rotational inertia of crushing device, ω_f is the crushing device rotation speed, k_f is the feed coefficient of crushing device.

Power demand of grain conveying

The churn, responsible for conveying cleaned grains to the grain tank, experiences active torque consisting of three components: the idling friction torque, the torque required for grain propulsion, and the moment of inertia associated with acceleration. The mathematical model describing the grain churn is formulated in Eq. (11).

$$P_h = \left(M_{df} + \frac{q_s k_{m1}}{367\omega_{d1}} k_{d1} L_d + \frac{q_s k_{m2} H_d}{367\eta_{hd}\omega_{d2}} + J_{d1}\frac{d\omega_{d1}}{dt} + J_{d2}\frac{d\omega_{d2}}{dt} \right)\omega_H \quad \text{(Eq. 11)}$$

where: P_h is the power demand of the grain conveying component, M_{df} is the idling friction torque, J_{d1}, J_{d2} are the rotational inertia of the horizontal churn and vertical churn, respectively, k_{m1}, k_{m2} are the seed mass feeding coefficient inside the horizontal churn and vertical churn, respectively, ω_{d1}, ω_{d2} are the rotation speed of the horizontal churn and vertical churn, respectively, k_{d1} is the conveying resistance coefficient, L_d is the length of the horizontal churn, H_d is the height of the vertical churn, η_{hd} is the conveying efficiency, ω_H is rotational speed of grain conveying shaft.

Power demand of walking system

The traveling system, which drives the harvester's movement, encounters various resistance forces, including road driving resistance, ground slope resistance, and wind resistance. Given the harvester's modest driving speed and the focus on flat field operations in this study, field driving resistance is considered the predominant factor in the modeling process. The dynamic model is formulated in Eq. (12).

$$F_t = m \times f_F + m\frac{dv}{dt} \quad \text{(Eq. 12)}$$

where: F_t is the harvester travel driving force, m is the total mass of the harvester, f_F is the rolling friction coefficient.

As the mass in the grain bin increases with operation time, the relationship between the harvester's mass and the feed rate is quantitatively established in Eq. (13).

$$m = m_{\text{combine}} + \int_0^t q_s \quad \text{(Eq. 13)}$$

where: m_{combine} is the unloaded mass of the harvester.

The power demand model of the travel system is shown in Eq. (14).

$$P_d = \frac{v_{combine} F_t}{\eta_d} \quad \text{(Eq. 14)}$$

where P_d is the power demand of the harvester travel system, v_{combine} is the harvester travel speed, η_d is the efficiency of the travel drive system.

Power demand of unloading system

The grain unloading system is independent of the feed rate, and the power demand can be taken as constant during the operation, as shown in Eq. (15).

$$P_u = T_u \omega_u \quad \text{(Eq. 15)}$$

where: P_u is power demand of the grain unloading system, T_u is the driving torque of the grain unloading, ω_u is the rotation speed of the grain unloading system.

Total power demand of components

The average power demand over the quasi-cycle is modeled by integrating the power demand models of key components, including harvesting, traveling, grain unloading, and heat dissipation. This comprehensive model is concisely formulated in Eq. (16).

$$P_{\text{quasi\_period}} = \frac{(P_g + P_s + P_t + P_q + P_h + P_d + P_f)t_r + 2P_d t_d + P_u t_u}{t_r + 2t_d + t_u} + P_{hd} \quad \text{(Eq. 16)}$$

where: $P_{\text{quasi\_period}}$ is the average power demand of the harvester during the whole quasi-cycle, t_r, t_d, t_u are the duration of harvesting process, transfer process and grain unloading process, respectively, P_{hd} is power of heat dissipation system.

Power management optimization strategy based on genetic algorithm

The power demand of the harvester during quasi-cycle operation is closely related to the volume of processed feed. Consequently, real-time adjustments to the power demand within the quasi-cycle are essential for efficient operation. The harvester's feed rate can be inferred from the dynamic responses of its components. Based on this feed rate estimation, an immediate correction of the power demand is calculated. Additionally, a genetic optimization algorithm has been developed to optimize the quasi-cycle process by refining the engine's operating points, specifically to enhance fuel consumption efficiency.

Power demand based on real-time feed rate estimation

The feed rate primarily affects the dynamics of the cutting table, conveying chute, and threshing drum in a harvester. According to the modeling equations discussed earlier, the kinetic characteristics of the conveying chute are only marginally influenced by factors such as land surface conditions and operating speed. As a result, the feed rate emerges as the dominant factor affecting the torque of the conveyor trough.

In this section, the conveying chute is selected as the basis for estimation. The feed rate is determined using the churn kinetic model (Liang *et al.*, 2024). The estimations for both the feed rate and the seed feed rate are formulated in Eqs. (17) and (18).

$$q_{e\_s} = \frac{\frac{P_s}{\omega_b} - M_{bi} - \frac{J_b}{i_b}\frac{d\omega_b}{dt}}{k_{sq} + \frac{k_{sm}}{i_b}\frac{d\omega_b}{dt}} \quad \text{(Eq. 17)}$$

$$q_{s\_e} = \frac{\frac{P_h}{\omega_H} - M_{df} - J_{d1}\frac{d\omega_{d1}}{dt} - J_{d2}\frac{d\omega_{d2}}{dt}}{\frac{k_{m1}}{367\omega_{d1}}k_{d1}L_d + \frac{k_{m2}H_d}{367\eta_d\omega_{d2}}} \quad \text{(Eq. 18)}$$

where: q_{s_e} is the seed feed estimation and q_e is the crop feed rate estimation.

Optimal control of range extender based on genetic algorithm

The estimated seed feed q_{s_e} and the estimated crop feed q_e were substituted into Eq. (16) to estimate the energy requirement of the quasi-cycle process, as shown in Eq. (19) (Lu *et al.*, 2020).

$$E'_{\text{quasi\_period}} = (P_{g\_qe} + P_{s\_qe} + P_{t\_qe} + P_{q\_qse} + P_{h\_qse} + P_{f\_qse} + P_d + P_f + P_r + P_{hd})$$

$$\frac{m_{\text{tank}}}{q_{s\_e}} + 2P_d t_d + P_u t_u + P_{hd}(2t_d + t_u)$$

(Eq. 19)

where: m_{tank} is the maximum mass of seed in grain bin, P_{g_qe}, P_{s_qe}, P_{t_qe}, P_{q_qe}, P_{h_qe}, P_{f_qe}, are estimated power demand of the header, conveying trough, threshing drum, cleaning device, grain conveying churn, crushing system under the corresponding feeding capacity respectively.

The complexity and nonlinear nature of optimizing engine operating points during the quasi-cycle require a sophisticated approach. To address this, a genetic algorithm (GA) is employed. The method involves discretizing the quasi-cycle period into 10-second intervals, serving as the foundation for allocating optimal operating power across various discretization steps to improve the algorithm's real-time performance. After discretization, the results are refined through linear interpolation, mapping the optimal power levels to their corresponding operating points to achieve the most efficient operational outcome (Lipowski and Lipowska, 2012).

Objective function: The GA primary objective is to minimize fuel consumption. The fitness function within the algorithm is specifically designed to achieve this goal.

Constraints: The constraints ensure compliance with the total energy demand of the process while enforcing upper and lower power limits. These constraints are formulated in Eqs. (20) and (21) and are incorporated into the algorithm's iterations using a penalty function.

$$(P_1 + P_2 \cdots P_N)\frac{t_{\text{discretized}}}{N} = E_{\text{quasi\_period}}\frac{N}{4} \quad \text{(Eq. 20)}$$

$$0 \le P_i \le P_{\max}(i = 1,2,3 \ldots N) \quad \text{(Eq. 21)}$$

where: $t_{\text{discretized}}$ is intervals time, $P_i(i = 1,2 \ldots N)$ are following population generation.

Gene coding: the GA employs binary coding for gene representation, where power levels are segmented and each segment is encoded as a binary number.

Initialization: The population size is set to N, with each individual's gene sequence also having a length of N, meaning that each individual represents a power allocation sequence for N nodes. The initial population is generated by randomly assigning power values within the predefined power range for each node, as formulated in Eq. (22).

$$0 \le P_{\text{initial\_i}} \le P_{\max}(i = 1,2 \ldots N) \quad \text{(Eq. 22)}$$

where: $P_{\text{initial\_i}}(i=1,2 \ldots N)$ are initial population generation, N is the number of intervals, $P_{\max}$ is the maximum power of extender.

Genetic manipulation: this involves selection, crossover, and mutation processes to create new individuals. Roulette wheel selection is used to prioritize individuals with lower objective values. Selection probabilities of all individuals are used to calculate the cumulative probability, as per Eq. (23). A random number e, ranging between 0 and 1, is generated and compared with the cumulative probability to select individuals. This process is repeated n times to create n offspring individuals.

$$S_l = \sum_{j=1}^{l} \frac{f_j}{\sum_{k=1}^{N} f_k} \quad \text{(Eq. 23)}$$

where: f_j *and* f_k are fitness of individual j and k, S_l is cumulative probability of individual l.

The random number e, which is between 0 and 1, is generated and compare with S_l to determine selection individual. If S_{m-1}<e< S_m, the no. m individual is selected. Repeated N rounds are conducted to generate N individuals of offspring generation. Repeat this process until the maximum number of iterations is reached or the objective function converges.

Simulation experiment design

To validate the effectiveness of the proposed algorithm, fuel-driven and hybrid harvester models were developed using Amesim and Simulink, as illustrated in Figures 4 and 5. These models played a crucial role in designing and evaluating various energy management strategies under different engine models and operational conditions.

To validate the algorithm's applicability across different equipment parameters, we employed two distinct engine models for verification: one derived from the Diesel_100kW model in Amesim, and the other based on the dynamometer external characteristic curve of YC-6B160Z engines. The corresponding parameters for these engine models can be found in Appendix C.

In the simulation process, two specific working conditions were selected: high feed rate and low feed rate scenarios. These scenarios were chosen to assess the algorithm's adaptability to varying operational demands. The crop types and corresponding parameters for both simulation cases are detailed in Table 2.

The study developed and compared three approaches: a speed-following strategy for the fuel-driven harvester, a power-following strategy for the hybrid harvester, and an energy management control strategy based on quasi-periodic power demand within the hybrid configuration. These strategies were rigorously simulated across various operational cycles to evaluate their impact on fuel consumption and the distribution of engine operating points.

To simplify the model, the following assumptions are defined for the simulation: it is assumed that the combine harvester maintains a stable speed under each operating condition and operates at full cutting width during harvesting, disregarding factors such as sudden changes in crop density or terrain that may affect the overall load. The study also neglects the impact of environmental factors (*e.g.*, temperature) on motor efficiency and battery energy loss.

Variables and their range of variation of the simulation are shown in Table 3.

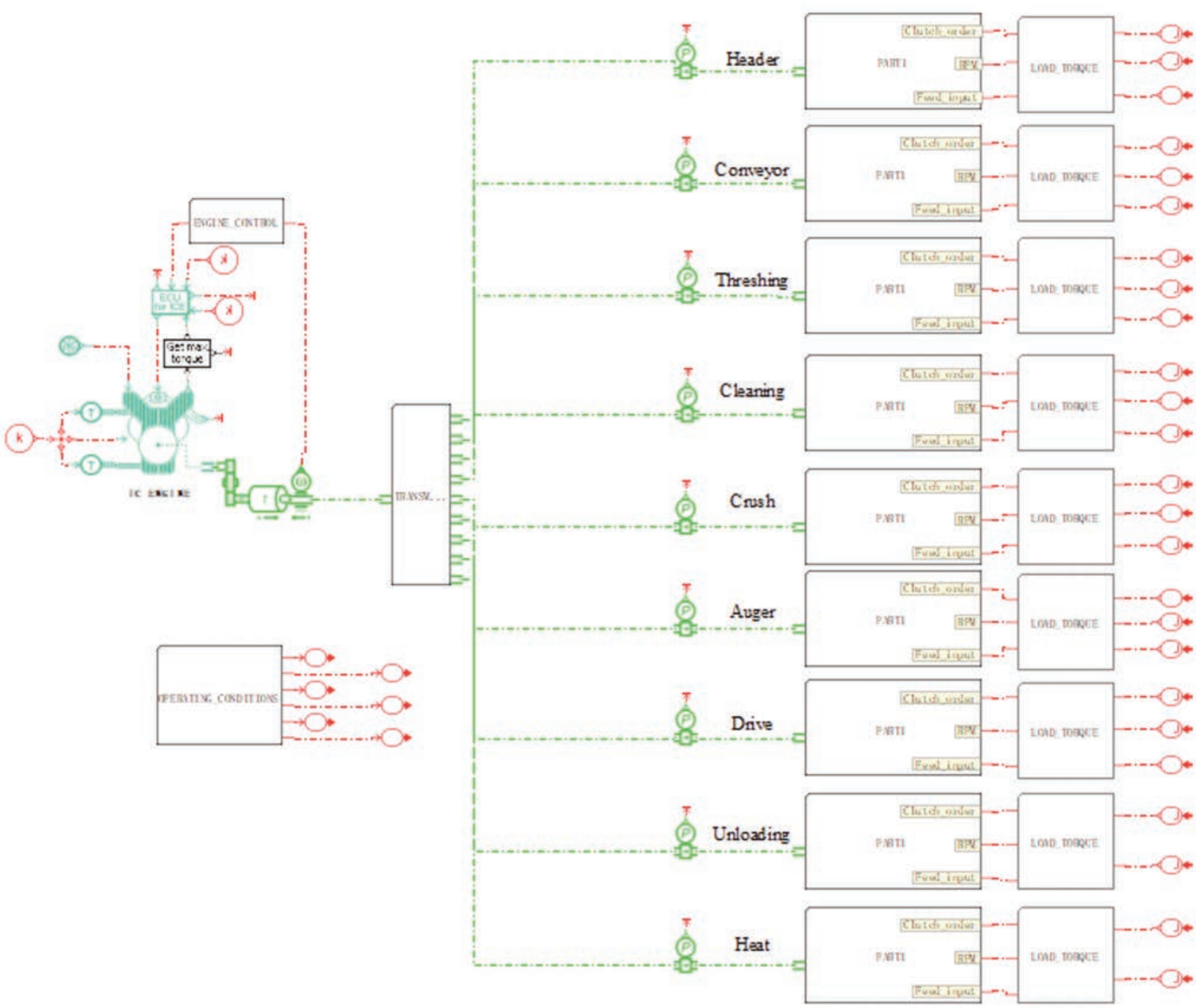

Figure 4. Model of fuel-driven combine harvester.

Results and Discussion

Figures 6 and 7 illustrate the operating points of two engine models (Diesel_100kW and YC-6B160Z) under the low feed rate test condition. The corresponding subfigures (a), (b), and (c) represent the engine speed and torque distribution under different configurations: fuel-driven configuration, hybrid configuration using the power-following strategy, and hybrid configuration employing the quasi-cycle strategy, respectively.

Figures 6 and 7 collectively illustrate the differences in engine speed and torque distribution between fuel-driven and hybrid harvesters. In fuel-driven configurations, the engine shaft is belt-connected to components, fixing the ratio between engine and component speeds. This constraint limits control over engine speed, clustering most operation points within four distinct zones corresponding to key harvesting processes: harvesting, full-load transferring, unloading, and empty-load transferring. Notably, fuel efficiency is lower during transferring and grain unloading. In contrast, hybrid harvesters decouple engine speed from component speed, allowing greater flexibility to optimize fuel consumption. Under the power-following strategy, engine power aligns with operational power at an optimal speed, enhancing fuel efficiency. The quasi-cycle energy management strategy further improves efficiency by estimating real-time feed rates to plan optimal operating points. This decoupling enables hybrid harvesters to maintain engine operation within higher efficiency zones, ensuring more effective power utilization. Although the two engines exhibit some differences in speed and torque performance, they share a common characteristic under this operating condition: the quasi-cycle energy management strategy distributes more operating points within the high-efficiency zone, which explains why this strategy achieves better fuel economy. Figures 8 and 9 illustrate that under high-feed conditions, the fuel-driven harvester's operation points during transferring and harvesting often fall into less efficient ranges, reducing overall fuel

Table 2. Scenario parameters description.

	Units	High feed rate test	Low feed rate test
Crop type	/	rice	rice
Feed rate	kg/s	9	3
Crop density	kg/m^2	1.3	1.3
Grain-to-straw ratio	/	0.81	0.81
Stubble height	cm	15	15
Operating speed	km/h	8.95	2.98

Table 3. Variables and their range of variation.

Variable	Unit	Range
Forward speed	km/h	1-9
Initial and final soc of battery	%	20-100
Engine speed	r/min	600-3000 (Diesel_100kW) 700-2200 (YC-6B160Z)
Engine torque	Nm	40-350 (Diesel_100kW) 100-580 (YC-6B160Z)
Range of specific fuel consumption	g/kwh	277.3-1005.4 (Diesel_100kW) 192.6-312.5 (YC-6B160Z)

Table 4. Comparison of fuel consumption.

Scenario/ engine model	Configurations and strategy	Total fuel consumption (g)	Fuel saving efficiency (%)	Initial SoC value (%)	Final SoC value (%)	Specific fuel consumption (kg/hm²)
Scenario 1/Diesel_100kW	Fuel-driven operating	6091.5	/	/	/	32.0
	Hybrid power-following	4413.8	27.5	60.0	60.1	23.2
	Hybrid quasi-cycle	4360.2	28.4	60.0	60.2	22.9
Scenario 2/ Diesel_100kW	Fuel-driven operating	3930.0	/	/	/	20.6
	Hybrid power-following	3799.6	3.3	60.0	60.1	20.0
	Hybrid quasi-cycle	3213.7	18.2	60.0	60.2	16.9
Scenario 1/ YC-6B160Z	Fuel-driven operating	3773.5	/	/	/	19.8
	Hybrid power-following	3188.9	15.5	60.0	60.4	16.7
	Hybrid quasi-cycle	3010.7	20.2	60.0	60.5	15.8
Scenario 2/ YC-6B160Z	Fuel-driven operating	2164.6	/	/	/	11.4
	Hybrid power-following	2075.9	4.1	60.0	60.1	10.9
	Hybrid quasi-cycle	2017.0	6.8	60.0	60.5	10.6

efficiency. In contrast, the hybrid harvester using the power-following strategy can adjust its speed to match real-time power demands. However, due to fluctuating power requirements, the optimal efficiency point frequently shifts outside the most efficient zone. The quasi-cycle power demand estimation strategy effectively decouples power demand by optimizing the engine's operating position based on the estimated average power demand over the entire cycle. This approach demonstrates superior energy-saving performance compared to the power-following-based energy management strategy in hybrid harvesters.

The effectiveness of these strategies in terms of total fuel consumption and fuel-saving efficiency is detailed in Table 4. This Table provide an overview of the fuel economy achieved under different operational conditions and strategies, highlighting the

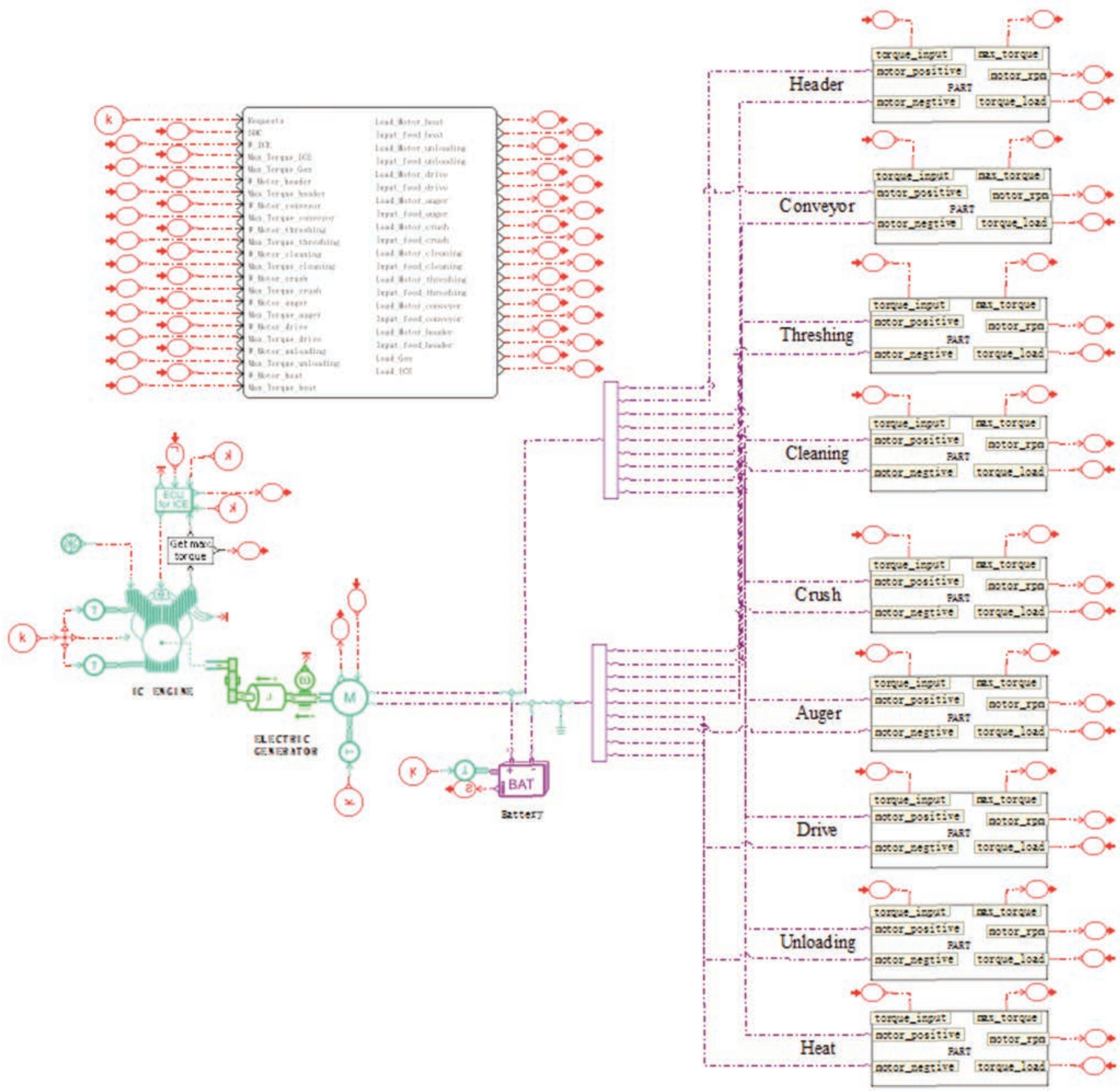

Figure 5. Hybrid distributed drive combine model.

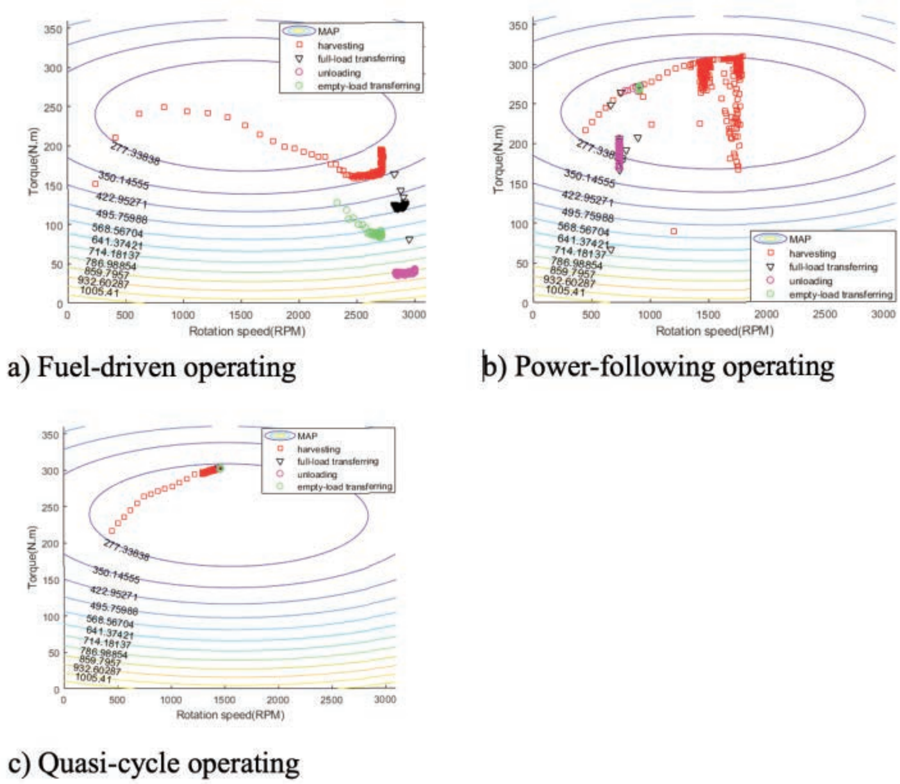

Figure 6. Operating points under low feed rate conditions with engine Diesel_100kW.

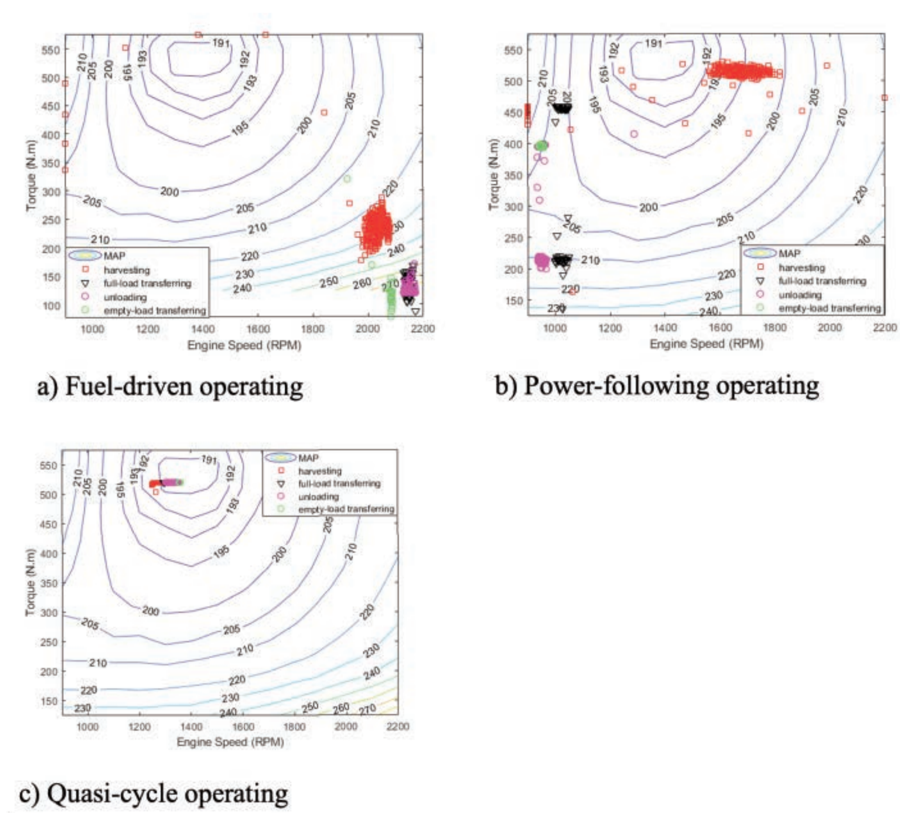

Figure 7. Operating points under low feed rate conditions with engine YC-6B160Z.

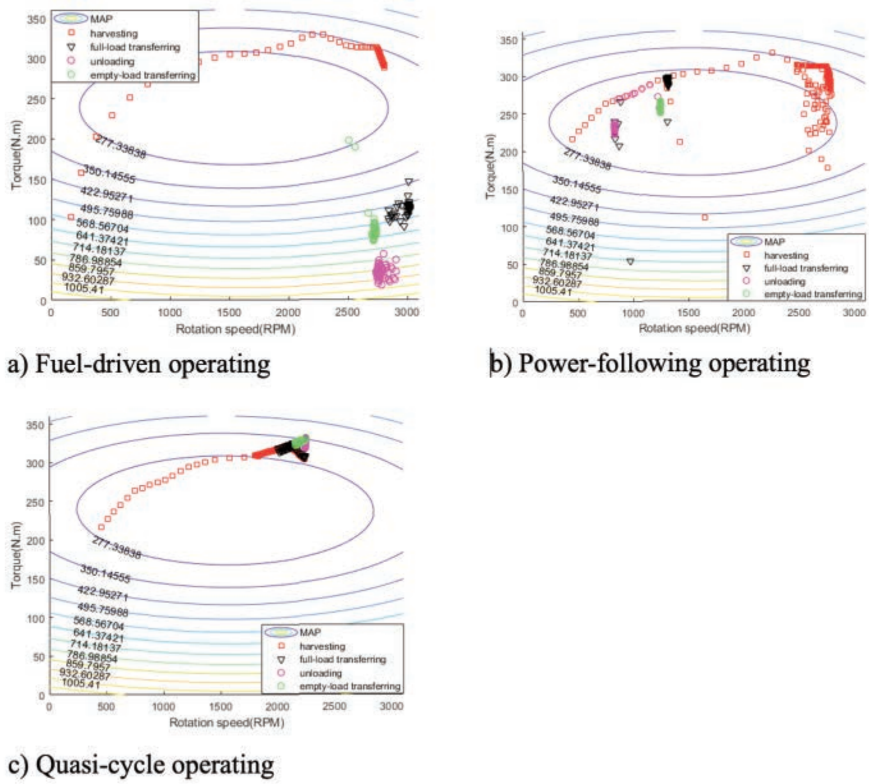

Figure 8. Operating points under high feed rate conditions with engine Diesel_100kW.

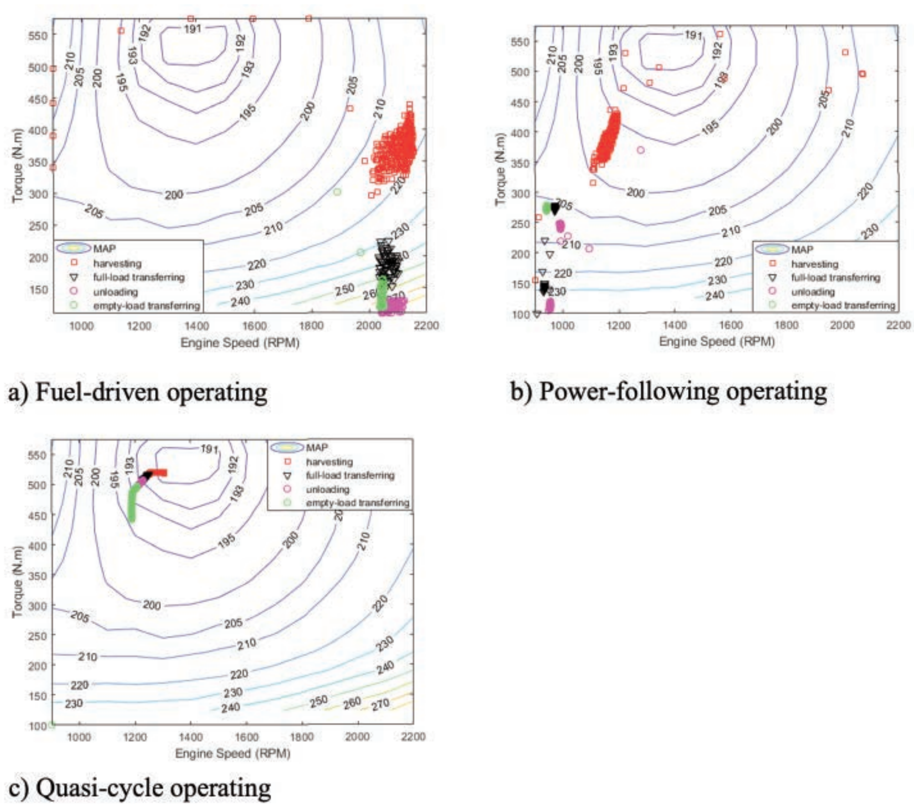

Figure 9. Operating points under high feed rate conditions with engine YC-6B160Z.

advantages of the quasi-periodic process power demand estimation in optimizing fuel efficiency. Compared to the fuel-driven operating, the quasi-cycle power demand estimation strategy significantly enhances fuel efficiency. Specifically, this strategy reduces fuel consumption by 21.1% compared to the fuel-driven harvester and 6.5% compared to the power-following strategy. These figures underscore the effectiveness of the quasi-cycle power demand estimation approach in optimizing fuel efficiency, marking a substantial improvement over both the conventional fuel-driven method and the power-following strategy.

Conclusions

This paper comprehensively analyzes the components of a harvester and their respective power demands to construct a detailed power demand model tailored for quasi-cycle harvester operations. The feed rate estimation is grounded in the dynamic responses of the harvester's components. Based on the estimation, the power demand characteristics of the quasi-cycle process are adjusted and refined. A genetic algorithm is employed to enhance energy efficiency further, focusing on optimizing fuel consumption by adjusting working points. This approach results in significantly improved energy performance.

Acknowledgements

This research was supported by Project of Faculty of Agricultural Engineering of Jiangsu University (NZXB20210103), the National Natural Science Foundation of China (52172346), CATARC Science and Technology Special 002 Project (30123003), MBSE simulation scenarios research project for BYD Automotive Industry Co., Ltd. (2022GG037), and Postgraduate Research & Practice Innovation Program of Jiangsu Province (KYCX18_2230) .

References

Ali, A.M., Moulik, B., 2022. On the role of intelligent power management strategies for electrified vehicles: a review of predictive and cognitive methods. IEEE Trans. Transp. Electr. 8:368-383.

Chai, X., Hu, J., Ma, T., Liu, P., Shi, M., Zhu, L., Zhang, M., Xu, L., 2024. Construction and characteristic analysis of dynamic stress coupling simulation models for the attitude-adjustable chassis of a combine harvester. Agronomy (Basel) 14:1874.

Chen, J., Ning, X., Li, Y., Yang, G., Wu, P., Chen, S., 2017. A fuzzy control strategy for the forward speed of a combine harvester based on KDD. Appl. Eng. Agr. 33:15-22.

Chen, J., Wang, Yifan, Wang, X., Wang, Yuehong, Hu, R., 2017. Development and application of remote video monitoring system for combine harvester based on embedded Linux. Proc. SPIE 10322. 17th Int. Conf. Electron. Inform. Eng. 1032223.

Deng, X., Yan, Z., Xu, D., Qi, Y., 2020. Land registration, adjustment experience, and agricultural machinery adoption: empirical analysis from rural China. Land (Basel) 9:89.

Guo, J., He, H., Sun, C., 2019. ARIMA-based road gradient and vehicle velocity prediction for hybrid electric vehicle energy management. IEEE Trans. Veh. Technol. 68:5309-5320.

Hu, J., Zong, C., Shi, M., Wang, L., Bi, Q., Xu, L., 2024. A robust ensemble surrogate model and its application in the in situ data modelling and analysis of a combine harvester. Engin. Optim. 56:1929-1949.

Kotenko, V., 2022. Method and results of the most efficient means of transport selection for executing orders of the grain crops delivery. Proc. Int. Conf. Transbaltica Transportation Science and Technology. Springer, pp. 606-617.

Lang, J., Tian, J., Zhou, Y., Li, K., Chen, D., Huang, Q., et al., 2018. A high temporal-spatial resolution air pollutant emission inventory for agricultural machinery in China. J. Cleaner Prod. 183:1110-1121.

Liang, Z., Qin, Y., Su, Z., 2024. Establishment of a feeding rate prediction model for combine harvesters. Agriculture (Basel) 14:589.

Lipowski, A., Lipowska, D., 2012. Roulette-wheel selection via stochastic acceptance. Physica A 391:2193-2196.

Liu, T., Tan, W., Tang, X., Zhang, J., Xing, Y., Cao, D., 2021. Driving conditions-driven energy management strategies for hybrid electric vehicles: A review. Renew. Sust. Energ. Rev. 151:111521.

Lu, E., Xu, L., Li, Y., Tang, Z., Ma, Z., 2020. Modeling of working environment and coverage path planning method of combine harvesters. Int. J. Agric. Biol. Eng. 13:132-137.

Luo, Y., Wei, L., Xu, L., Zhang, Q., Liu, J., Cai, Q., Zhang, W., 2022. Stereo-vision-based multi-crop harvesting edge detection for precise automatic steering of combine harvester. Biosyst. Engin. 215:115-128.

Savickas, D., Steponavičius, D., Kliopova, I., Saldukaitė, L., 2020. Combine harvester fuel consumption and air pollution reduction. Water Air Soil Pollut. 231:95.

Schmid, R., Bürger, J., Bajcinca, N., 2019. A comparison of PMP-based energy management strategies for plug-in-hybrid electric vehicles. IFAC Papersonline 52:592-597.

Shi, D., Guo, J., Liu, K., Cai, Q., Wang, Z., Qu, X., 2023. Research on an improved rule-based energy management strategy enlightened by the DP optimization results. Sustainability (Basel) 15:10472.

Shi, D., Liu, S., Cai, Y., Wang, S., Li, H., Chen, L., 2021. Pontryagin's minimum principle based fuzzy adaptive energy management for hybrid electric vehicle using real-time traffic information. Appl. Energ. 286:116467.

Shi, D., Pisu, P., Chen, L., Wang, S., Wang, R., 2016. Control design and fuel economy investigation of power split HEV with energy regeneration of suspension. Appl. Energ. 182:576-589.

Sun, L., Liu, M., Wang, Z., Wang, C., Luo, F., 2023. Research on load spectrum reconstruction method of exhaust system mounting bracket of a hybrid tractor based on MOPSO-wavelet decomposition technique. Agriculture (Basel) 13:1919.

Sun, Y., Liu, R., Zhang, M., Li, M., Zhang, Z., Li, H., 2022. Design of feed rate monitoring system and estimation method for yield distribution information on combine harvester. Compute. Electron. Agr. 201:107322.

Wang, C., Huang, B., Xu, W., 2018. An integrated energy management strategy with parameter match method for plug-in hybrid electric vehicles. IEEE Access 6:62204-62214.

Wang, S., Zhang, S., Shi, D., Sun, X., Yang, T., 2021. Research on hybrid modeling and predictive energy management for power split hybrid electric vehicle. Bull. Pol. Acad. Sci. 69:e137064.

Wang, Y., Li, K., Zeng, X., Gao, B., Hong, J., 2023. Investigation of novel intelligent energy management strategies for connected HEB considering global planning of fixed-route informa-

tion. Energy 263:125744.
Xu, L., Li, Yang, Chai, X., Wang, G., Liang, Z., Li, Yaoming, Li, B., 2020. Numerical simulation of gas–solid two-phase flow to predict the cleaning performance of rice combine harvesters. Biosyst. Engin. 190:11–24.
Xuegeng, C., Haojun, W.E.N., Weirong, Z., Fochu, P.A.N., Yan, Z., 2020. Advances and progress of agricultural machinery and sensing technology fusion. Smart Agr. 2:16.
Yang, T., Zhao, L., Li, W., Zomaya, A.Y., 2021. Dynamic energy dispatch strategy for integrated energy system based on improved deep reinforcement learning. Energy 235:121377.
Yu, H., Kuang, M., McGee, R., 2013. Trip-oriented energy management control strategy for plug-in hybrid electric vehicles. IEEE Tr. Control Syst. Technol. 22:1323-1336.
Yun, Q., Dean, Z., Wei, J., 2010. Combines speed servocontrol based on gray generalized predictive algorithm. Proc. IEEE Int. Conf. on Computer, Mechatronics, Control and Electronic Engineering. pp. 21-24.
Zhang, F., Hu, X., Langari, R., Cao, D., 2019. Energy management strategies of connected HEVs and PHEVs: Recent progress and outlook. Prog. Energ. Combust. 73:235-256.
Zhu, D., Pritchard, E., Dadam, S., Kumar, V., Xu, Y., 2021. Optimization of rule-based energy management strategies for hybrid vehicles using dynamic programming. Combust. Engin. 184:3-10.
Zhu, Z., Chai, X., Xu, L., Quan, L., Yuan, C., Tian, S., 2023. Design and performance of a distributed electric drive system for a series hybrid electric combine harvester. Biosyst. Engin. 236:160–174.
Zhu, Z., Zeng, L., Chen, L., Zou, R., Cai, Y., 2022. Fuzzy adaptive energy management strategy for a hybrid agricultural tractor equipped with HMCVT. Agriculture (Basel) 12:1986.

Online supplementary materials:
Appendix A. Key parameters of harvester.
Appendix B. Parameters of harvester system components and power units.
Appendix C. Parameters of the two engine models.